REPRINT

ChemistrySelect

Full Papers
doi.org/10.1002/slct.202002030

Chemistry
Europe
European Chemical
Societies Publishing

■ Catalysis

Surfactant Intercalated Mono-metallic Cobalt Hydrotalcite: Preparation, Characterization, and its Bi-functional Electrocatalytic Application

Dhanjay Sharma,[a] A. Sakthivel,*[b] S. Michelraj,[c, d] A. Muthurasu,[c, d] and V. Ganesh*[c, d]

A series of surfactants are intercalated into mono-metallic hydrotalcite type α-Co(OH)$_2$ through ion exchange method to produce organic-cobalt hydrotalcite (HT-SDS, HT-TMA and HT-SL). The resultant material maintains its inner laminate structure with increased interlayer spacing. FT-IR spectroscopic studies and powder XRD analysis revealed the successful intercalation of SDS into the interlayers of α-cobalt hydroxides. TEM and N$_2$ sorption studies further demonstrate the intercalation of organic surfactant in the interlayer spacing of CoHT. XPS studies indicated the presence of surface exposed cobalt in both Co^{2+} and Co^{3+} oxidation states. Furthermore, the applicability of these intercalated materials in electrocatalytic applications specifically for oxygen evolution reaction (OER) and oxygen reduction reaction (ORR) in alkaline medium is explored. Among the various investigated materials, sodium dodecyl sulphate (SDS) intercalated material exhibited better performance in terms of higher catalytic current at a lower overpotential value. Moreover, the kinetic parameters associated with electrocatalysis are determined, and the mechanism behind OER and ORR is elucidated. These results clearly demonstrate the potential bi-functional utility of such layered materials for electrocatalytic applications.

1. Introduction

Chemistry behind the intercalation of organic molecules into layered materials is very interesting and mainly involves host-guest interaction between the layered inorganic materials and organic macromolecules. This strategy often significantly changes the chemical, catalytic, adsorption, magnetic, optical, and electronic properties of the resultant intercalated layered materials.[1] The presence of organics within the interlayer of inorganic materials facilitates the isolation of active sites, which presents many opportunities for industrial applications such as heterogeneous catalysts, adsorbents to remove toxic effluents, and in electrochemical devices such as capacitors, sensors, electrocatalysts and batteries.[2] Nanoporous inorganic materials such as clay (cationic and anionic) and layered zeolites play a major role in the intercalation of several ionic and non-ionic

molecules.[3] Hydrotalcite (HT) is one of the attractive candidates that possess exchangeable anions that can intercalate into the interlayer space forming a variety of composite materials.[4,5] The introduction of various anions such as inorganic ions, polyoxo anions, and organic anions, along with macromolecules impart unique properties to the composite, which render them promising applications in various fields namely adsorption, catalysis, polymer additives, drug delivery, supercapacitors, electro-catalysis, bio-sensors, and optical devices.[4,5]

Layered hydrotalcite materials are positively charged, with anionic (e.g. SiO$_4$$^{4-}$, CO$_3$$^{2-}$, NO$_3$$^{2-}$, Cl$^-$, and OH$^-$) gallery occupying the interlayer spacing.[5] Different layered materials have been studied with the intercalation of various anionic surfactants. Mg—Al LDH (layered double hydroxide) materials have been reported with intercalating ions, viz., SDS, sulfate, sulfonate, carboxylate, and phosphate; the resultant materials find various applications as the polymer nanocomposites and lubricant additives.[6] In addition, recent years attention also focused on the preparation of mono-metallic hydrotalcite and explored its applications.[4b,c and 5b,c] In this regard, it is worth mentioning here that, cobalt hydroxide exists in two polymorphs viz., α-Co(OH)$_2$ and β-Co(OH)$_2$, among which α-Co(OH)$_2$ is difficult to synthesize because the α-phase is meta-stable and transforms rapidly into the β-form during synthesis.[5] α-Hydroxides are isostructural with hydrotalcite-like materials. In general, mono-metallic HT derived from α-Co(OH)$_2$ exhibits superior electrochemical activity as compared to that of the β-form because of its poor or turbo-statically crystallized structure.[7] Hence, the anionic surfactant-intercalated cobalt layered double hydroxides with large interlayer spacing have attracted much interest for the study of electrochemical redox activity, mineral flotation

[a] Dr. D. Sharma
     Department of Chemistry, Inorganic Materials & Catalysis Laboratory,
     University of Delhi (North Campus), Delhi-110007, India
     E-mail: dhananjay.ssd@gmail.com
[b] Prof. Dr. A. Sakthivel
     Department of Chemistry, School of Physical Sciences, Central University
     of Kerala, Tejaswini Hills, Periye P.O., Kasaragod-671320, Kerala, India
     E-mail: sakthiveldu@gmail.com
          sakthivelcuk@cukerala.ac.in
[c] S. Michelraj, Dr. A. Muthurasu, Dr. V. Ganesh
     Electrodics and Electrocatalysis (EEC) Division, CSIR – CentralElectrochem-
     ical Research Institute (CSIR–CECRI), Karaikudi – 630003, Tamilnadu, India.
[d] S. Michelraj, Dr. A. Muthurasu, Dr. V. Ganesh
     Academy of Scientific and Innovative Research (AcSIR), Ghaziabad –
     201002, India
     E-mail: vganesh@cecri.res.in
          ganelectro@gmail.com

ChemistrySelect

Full Papers
doi.org/10.1002/slct.202002030

Chemistry Europe
European Chemical
Societies Publishing

in detergency, and dispersion/flocculation etc.[7] Due to the strong hydrophobic interactions among the long chains of surfactants, they are selectively intercalated into the layered materials.[8]

Oxygen evolution reaction (OER) and oxygen reduction reaction (ORR) electrocatalysts play a vital role in the energy conversion of fuel cell and metal air batteries. Noble metal based electrocatalysts namely Pt, IrO_2 and RuO_2 act as the state of art/benchmark catalysts for OER and ORR at present. But due to their limited availabity and high cost, they suffer from commercialization.[9] Hence, the development of other catalysts comprising of cheaper, earth abundant materials for performing efficient OER and ORR attaracted recent research across the globe. Among the other materials, transition metal based compounds consisting of oxides, metal hydroxides and oxy-hydroxides have received more attention and these materials were widely studied in the recent years.[10–16] Co in the form of CoO, Co_3O_4, Co_3Se_4, Co_9S_8 and CoP were shown to possess good catalytic activity and stability for both OER and ORR in alkaline medium.[10–16] Among these, α-Co(OH)$_2$ is more attractive because of the structural diversity and cost effectiveness for further scale up.

Keeping this in mind, in this work, we investigated the intercalation of a series of organic anions such as sodium dodecyl sulfate (SDS, $C_{12}H_{25}OSO_3Na$), trimesic acid (TMA), sodium laureate (SL) into the interlayer space of mono-metallic hydrotalcite type α-Co(OH)$_2$ (Scheme 1). The structural, morphological, and intrinsic properties of the resultant materials are analyzed using physico-chemical and analytical methods (FT-IR, powder XRD, XPS, TGA, BET and TEM). The introduction of organic surfactant provides a hydrophobic environment and increases the interlayer spacing. Further, these materials are explored for electrocatalytic applications. The results clearly reveal that SDS intercalated Co-HT acts as a potential bi-functional electro-catalyst for OER and ORR in alkaline medium. Several kinetic parameters associated with the electro-catalytic processes are also determined.
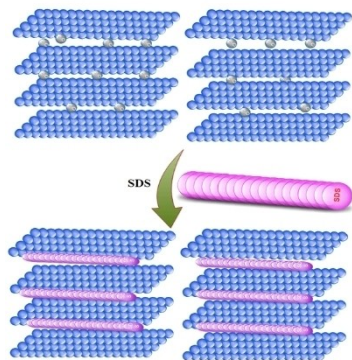
2. Results and discussion

Basically, in this work various surfactants intercalated hydro-talcite type α-Co(OH)$_2$ materials are prepared and characterized. The α-Co(OH)$_2$ intercalated with sodium dodecyl sulfate (0.5 and 1.0 mmol), trimesic acid (1.0 mmol) and sodium laurate (1.0 mmol) are represented as HT-SDS-1, HT-SDS-2, HT-TMA-1 and HT-SL-1 respectively.

Further these materials are explored for OER and ORR applications associated with alkaline water spilitting reaction. Figure 1 shows the FT-IR spectra of as-prepared α-Co(OH)$_2$ and different anionic surfactants intercalated cobalt hydrotalcite. The peaks corresponding to -OH stretching mode of interlayer water molecules and bending mode of water molecules are observed around 3450 cm^{-1} and 1610 cm^{-1}, respectively.[17] The formation of α-phase cobalt hydroxide is well supported by the FTIR spectral studies based on the absence of a sharp peak near 3600 cm^{-1}, which is characteristic of the β-phase.[5] The characteristic vibrational bands of carbonate ions appeared at $\sim$ 850, 1048, 1350, and 1414 cm^{-1}. The vibrational bands observed at 667 and 470 cm^{-1} are associated with the Co—O stretching and Co-OH bending vibrations, respectively. [5,17]

In addition, the SDS-intercalated layered cobalt HT material showed the peaks around 2850–2920 cm^{-1} and 1210–1240 cm^{-1} along with a broad band around 1000 cm^{-1} due to the S=O stretching vibrations of the SO_4 group from the surfactant.[5,18] The strong peak at 2920 cm^{-1} can be attributed to alkyl chains, thus confirming the presence of surfactant, SDS.[18] Similarly, trimesic acid (TMA) and sodium laurate (SL) intercalated materials showed characteristic asymmetric and symmetric stretching C-H bands at around 1556 cm^{-1} and 1405 cm^{-1}, respectively, confirming their intercalation as well.[6]

Figure 2 shows the powder XRD patterns of HT type α-Co (OH)$_2$ and different anionic surfactant-intercalated cobalt hydrotalcite materials. The XRD profile of α-Co(OH)$_2$ displays four peaks at 8.26, 15.8, 33.61, and 60°, which correspond to (003), (006), (100), and (110) planes of the layered HT structure respectively.[19] The 'saw-tooth' peak at the 2θ value of 33.61° is
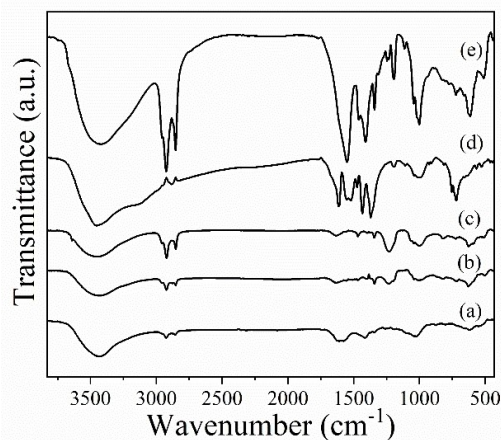

Scheme 1. Schematic representation of SDS intercalation into Co-Hydrotalcite.

Figure 1. FT-IR spectra of (a) α-Co(OH)$_2$, (b) HT-SDS-1, (c) HT-SDS-2, (d) HT-TMA-1 and (e) HT-SL-1 respectively.

ChemistrySelect

Full Papers
doi.org/10.1002/slct.202002030

Chemistry
Europe
European Chemical
Societies Publishing

Figure 2. Powder XRD patterns of (a) α-Co(OH)$_2$, (b) HT-SDS-1, (c) HT-SDS-2, (d) HT-TMA-1 and (e) HT-SL-1 respectively.

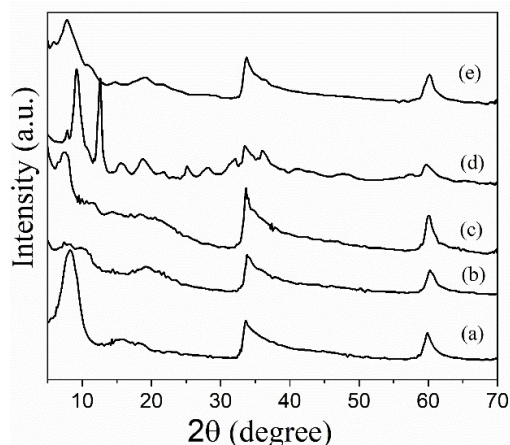**Figure 3.** N$_2$ adsorption-desorption isotherms of (a) α−Co(OH)$_2$, (b) HT-SDS-1, (c) HT-SDS-2, (d) HT-TMA-1 and (e) HT-SL-1 respectively.

due to the two-dimensional reflection of turbo-statically disordered α-Co(OH)$_2$.[6,19] The (110) peak indicates the internal laminated structure of the brucite-like layers.[19,20] In anionic surfactant-intercalated cobalt hydrotalcite, the shifting of *2θ* values to lower angles provides evidences for the intercalation of surfactants (SDS, TMA, and SL) into the interlayer spaces. Further, the decrease in intensity of the surfactant intercalated HT type α-Co(OH)$_2$ is attributed to the presence of organic intercalation between the interlayer space. The line broadening of X-ray reflections and shift in *2θ* values to lower angles are more prominent in case of SDS [(b) & (c)] compared to other organic anions, which support the presence of sulphate anions facilitate a strong interaction with cationic framework mono-metallic HT type α-Co(OH)$_2$. In particular, the use of organic anions trimesic acid is not effectively intercalated which is evident from the additional peak that appears around *2θ* value of 13.9° and may be due to acetate ion deposited in the interlayer and present as cobalt acetate impurities.[21]

Further, the results of N$_2$ adsorption-desorption analysis are displayed in Figure 3 and data are summarized in Table 1. Pure α-Co(OH)$_2$ showed a weak adsorption with H4-type hysteresis according to IUPAC,[22] corresponding to narrow slit-like pores present in the interlayer spacing of α-Co(OH)$_2$. The absence of such a hysteresis for organic-intercalated Co-HT confirms the presence of organics in the interlayer spacing of HT. This is further evidenced from the textural properties shown in Table 1. The BET surface area and pore volume of the as-
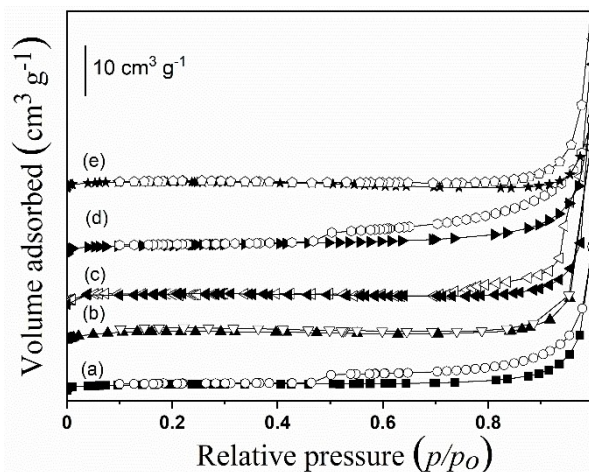
synthesized α-Co(OH)$_2$ are determined to be 14.21 m^2/g and 0.15 cm^3/g, respectively. In case of surfactant-intercalated materials, the surface area decreased owing to the presence of organics within the interlayer spacing of Co-HT. BJH curves of α-Co(OH)$_2$ and organic-intercalated Co-HTs showed broad non-uniform pore size distribution (Figure S1).

Furthermore, to understand the morphology of surfactant intercalated Co-HT, TEM investigations of SDS-intercalated Co-HT (HT-SDS-1 and HT-SDS-2) were carried out, and the corresponding images are displayed in Figure 4. Both the samples showed flocculation of HT particles with uniform ultra-thin two-dimensional needle-shaped HT structures (Figure 4a & 4b). Moreover, elemental analysis of all these samples (Table S1) showed the presence of all the expected elements and confirms the intercalation of surfactants into Co-HT materials.

XPS studies were performed to analyze the presence of elements and their corresponding oxidation states in both HT-SDS-1 and HT-SDS-2. The XPS core level spectra of Co 2p of these compounds shown in Figure 5 exhibit two main peaks (2p$_{3/2}$ and 2p$_{1/2}$) and two satellite peaks. Similarly, O 1s spectra of these samples are displayed in Figure 6. These surface charge compensated resultant spectra were deconvoluted using the Fityk (version 0.9) software and fitted with Gaussian-Lorentzian distribution to quantify the different oxidation states present in the materials; the results are summarized in Table 2.

Table 1. Textural properties of α−Co(OH)$_2$, HT-SDS-1, HT-SDS-2, HT-TMA-1 and HT-SL-1.					
S. No.	Sample code	Surface area (m^2/g)		Pore volume (cm^3/g)	
		BET	Micropore t-plot	BET	Micropore t-plot
1	α-Co(OH)$_2$	14.21	6.73	0.15	0.003
2	HT-SDS-1	5.04	4.24	0.05	0.002
3	HT-SDS-2	13.07	5.31	0.14	0.002
4	HT-TMA-1	23.6	7.95	0.16	0.004
5	HT-SL-1	13.9	3.6	0.05	0.001

ChemistrySelect

Full Papers
doi.org/10.1002/slct.202002030

Chemistry Europe
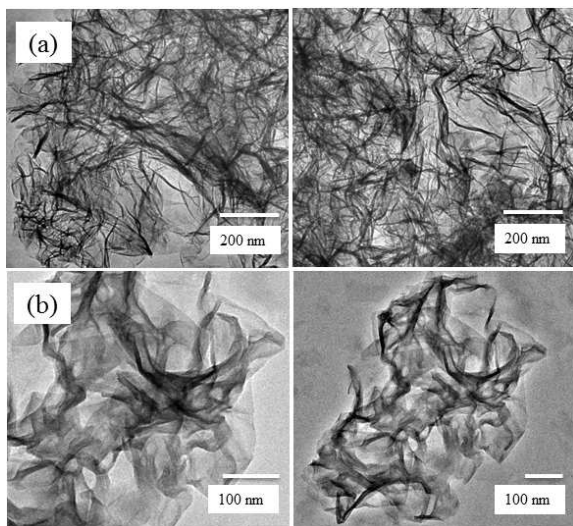European Chemical
Societies Publishing

Figure 4. TEM images of HT-SDS-1 (a) and HT-SDS-2 (b) recorded at different locations of the samples.
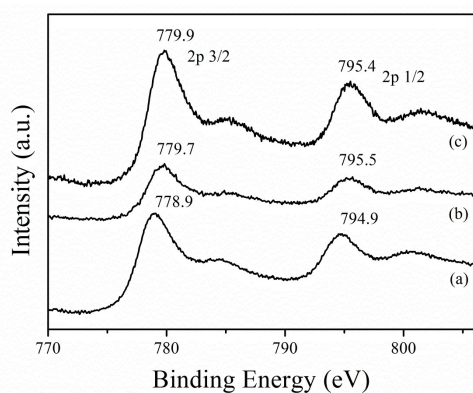

Figure 5. XPS data corresponding to Co 2p region of (a) α-Co(OH)$_2$, (b) HT-SDS-1 and (c) HT-SDS-2.
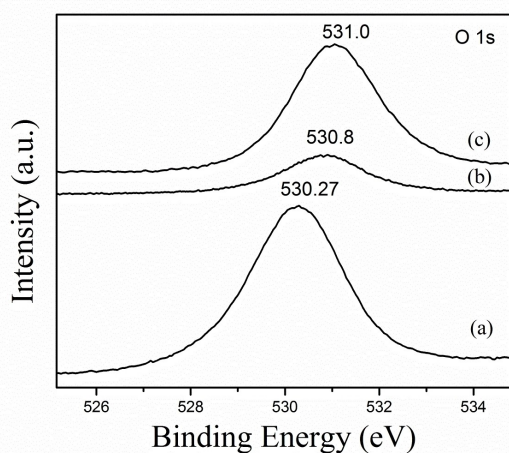

Figure 6. XPS data corresponding to O 1s region of (a) α-Co(OH)$_2$, (b) HT-SDS-1 and (c) HT-SDS-2.

The deconvoluted XPS data of Co 2p (Figure S2) of the α-phase materials showed a major peak at 778.9 eV and a less intense peak at 794.4 eV, which are typical of cobalt present in both Co^{2+} and Co^{3+} oxidation states (difference between 2p$_{3/2}$ and 2p$_{1/2}$ is 16.0 eV). In the case of surfactant-intercalated (HT-SDS-1 and HT-SDS-2) materials, the spin orbital splitting decreases from 16.0 eV to 15.8 and 15.5 eV, respectively, which indicates a relatively higher percentage of cobalt in the +3 oxidation state.[23] Thus, the resultant organic-intercalated Co-HT possesses the surface exposed cobalt in the Co^{3+} oxidation state. Further O 1s peak of α-Co(OH)$_2$ appeared at 530.27 eV and upon intercalation with surfactant this particular peak is shifted to a slightly higher binding energy of 530.8 eV and 531 eV in the case of HT-SDS-1 and HT-SDS-2 respectively. These observations indicate a marginal change in oxygen environment due to the intercalation of surfactant and presence of cobalt spinel species, which is clearly evident from deconvoluted spectra (Figure S3). The deconvoluted O 1s spectra showed the presence of CoO(OH) type species as a major component. Nevertheless, XPS results clearly show the presence of different elements confirming the purity of these samples and the existence of elements with different oxidation states.

3. Bi-functional electrocatalytic applications of surfactant intercalated Co-HT materials

Further the surfactant intercalated Co-HT materials are explored for electrocatalytic applications especially in the field of water splitting reaction predominantly for OER and ORR. These reactions play a vital role in energy conversion devices mainly in alkaline fuel cells. In order to investigate the electrocatalytic properties of different materials prepared in this work (namely HT-SDS-1, HT-SDS-2, HT-TMA-1, HT-SL-1 and pure α-Co(OH)$_2$), voltammetric studies such as linear sweep voltammetry (LSV) and cyclic voltammetry (CV) are carried out in 0.1 M KOH aqueous solution. Initially as-prepared catalytic ink was drop casted onto a pre-cleaned glassy carbon electrode and allowed to dry overnight. Interestingly among the various materials studied using electrochemical techniques only SDS intercalated Co-HT showed promising application as a catalyst for OER and ORR (Figures S4 & S5). Hence for the subsequent studies we employ HT-SDS-1 and HT-SDS-2 along with pure α-Co(OH)$_2$ for comparative purpose (results discussed later). Further the electrochemical interfacial characteristics of these materials are assessed using impedance measurements and the corresponding Nyquist plots are shown in figure S6. These studies are carried out at the open circuit potential of the respective material over a frequency ranging from 100 kHz to 100 mHz with a small sinusoidal voltage of 10 mV amplitude. It can be noted from these impedance plots that a small semicircle is formed at the high frequency region and a straight line is formed at low frequency region. This behaviour is a typical characteristic of diffusion-controlled process. A parameter namely, charge transfer resistance (R$_{ct}$) that represents the resistance offered by the electrode towards charge transfer process is determined from the equivalent circuit fitting

ChemistrySelect

Full Papers
doi.org/10.1002/slct.202002030

**Chemistry
Europe**
European Chemical
Societies Publishing

Sample code	Co 2p$_{3/2}$ (eV) Main	Satellite	Co 2p$_{1/2}$(eV) Main	Satellite	Spin orbital splitting (eV)	Co 2p$_{3/2}$ (eV)	Co 2p$_{1/2}$ (eV)
$\alpha-Co(OH)_2$	778.9	784.4	794.9	800.8	16.0	5.5	5.9
HT-SDS-1	779.7	785.4	795.5	801.4	15.8	5.7	5.9
HT-SDS-2	779.9	785.4	795.4	801.6	15.5	5.5	6.2

Table 2. XPS data of $\alpha-Co(OH)_2$, HT-SDS-1 and HT-SDS-2.

procedure. In this work, we employed a modified Randles equivalent circuit (Figure S6) comprising of a solution resistance (R$_s$) connected in series with a parallel combination of constant phase element (Q) and series assembly of R$_{ct}$ and Warburg (W) impedance. Using this, R$_{ct}$ values of 9809 Ω, 8204 Ω and 3822 Ω are determined for $\alpha-Co(OH)_2$, HT-SDS-1 and HT-SDS-2 respectively. Among these surfactants intercalated materials HT-SDS-2 exhibits a lower R$_{ct}$ indicating the better electrochemical interfacial characteristics. These results demonstrate the ability of these materials to be used for electrochemical applications.

In case of OER, LSV studies were performed for all these materials in 0.1 M KOH aqueous solution at a fixed scan rate of 5 mV/s and the corresponding voltammograms were displayed in figure 7A. For comparison similar LSV studies carried out using bare glassy carbon electrode without any modification was also shown as'd' (blue curve; inset 7 A). It can be seen from this figure that in contrast to bare glassy carbon electrode where there is no significant current due to OER, all the surfactant intercalated Co-HT materials show a significant enhancement in the current density due to OER. Among the

various catalysts studied HT-SDS-2, displayed a massive enhancement of about more than 60 fold increase in the current density when compared to HT-SDS-1 and pure α-Co(OH)$_2$. Moreover the onset potential values are determined to be 1.62 V, 1.63 V and 1.42 V for HT-SDS-2, HT-SDS-1 and α-Co(OH)$_2$ respectively. These values are more anodic when compared to the thermodynamic potential of 1.23 V vs. RHE for OER. Both HT-SDS-1 and HT-SDS-2 showed over-potential values of 400 mV and 390 mV for OER in alkaline medium respectively. On the other hand, α-Co(OH)$_2$ displayed an over potential value of 190 mV for OER. The potential value required to obtain a current density of 10 mA/cm^2 is commonly used to access the merit of any electrocatalyst. Particularly in this work, only HT-SDS-2 exhibits more than 10 mA/cm^2 current density when compared to other two materials and specifically this material showed a potential of 1.78 V vs. RHE is needed to obtain 10 mA/cm^2 current density. From these studies it is clear that HT-SDS-2 exhibits a higher oxidation current density at a lower onset potential for OER. Hence, Tafel polarization curves were recorded for this material and the corresponding Tafel plot is shown in figure 7B. These data points were collected using chronoamperometric studies in which the steady state current values were measured for change in overpotential values. A linear variation of current density with respect to increase in overpotential is noticed from Figure 7B and from this plot a Tafel slope of 61 mV/dec is determined. This lower Tafel slope value and higher electrocatalytic current density clearly indicate that HT-SDS-2 can be used for OER in alkaline medium. Better OER activity of HT-SDS-2 could be attributed to the layered structure and its enhanced surface area. From these studies the order of increased electrocatalytic activity of OER is found to be HT-SDS-1 $< \alpha$-Co(OH)$_2 <$ HT-SDS-2. In order to understand the stability of the best electrocatalyst namely HT-SDS-2 towards OER in alkaline medium the chronoamperometry curve was recorded and shown in figure 7C. This study was carried out by measuring the change in current density at a fixed potential of 1.8 V vs. RHE for about 10 hours. It can be noted that the catalyst retains 95% of the current for OER upto 4 hours and it decreased to 50% by 10 hours. These studies clearly demonstrate the good stability of the electrocatalyst towards OER in alkaline medium.

Furthermore, electrocatalytic activity of these surfactant intercalated materials toward ORR performance is also evaluated using LSV. These studies were carried out using 0.1 M KOH aqueous solution under N$_2$ and O$_2$ saturated conditions within the potential range of 0 V to -1.0 V vs. Ag/AgCl at a fixed scan rate of 10 mV/s. The corresponding linear sweep voltammograms are shown in figure 8. In this figure (a), (b) and (c)
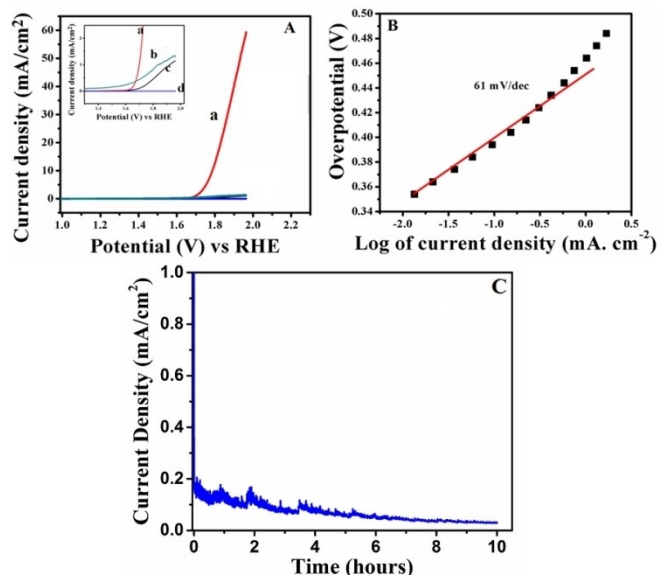

Figure 7. (A) LSV plots of HT-SDS-2 (a), pure α-Co(OH)$_2$ (b), HT-SDS-1 (c), and bare glassy carbon (d), electrodes respectively in 0.1 M KOH aqueous solution at a fixed scan rate of 5 mV/s and inset graph is the zoomed version of figure A. (B) The corresponding Tafel plot of HT-SDS-2, obtained for OER in 0.1 M KOH aqueous solution. (C) Chronoamperometric curve recorded at a fixed potential of 1.8 V for 10 hours to understand the stability of HT-SDS-2 towards OER in 0.1 M KOH solution.
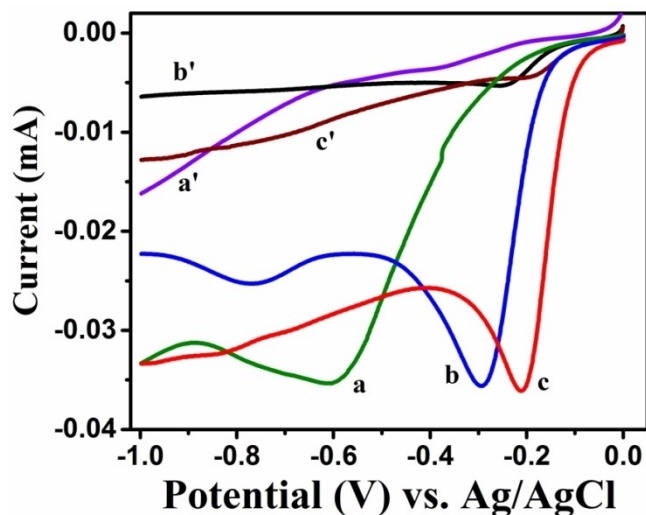
ChemistrySelect

Full Papers
doi.org/10.1002/slct.202002030

Chemistry Europe
European Chemical
Societies Publishing

Figure 8. LSVs recorded for ORR using (a) α-Co(OH)$_2$, (b) HT-SDS-1 and (c) HT-SDS-2 coated glassy carbon electrodes under O$_2$ saturated 0.1 M KOH aqueous solution at a fixed scan rate of 10 mV/s. Similarly, (a'), (b') and (c') designate the LSV curves recorded for these materials under N$_2$ saturated condition.

represent the LSV curves recorded for α−Co(OH)$_2$, HT-SDS-1 and HT-SDS-2 coated glassy carbon electrodes under O$_2$ saturated conditions respectively. Similarly, (a'), (b') & (c') denote the corresponding LSV curves obtained under N$_2$ saturated condition for these materials. It can be seen from these voltammograms that the formation of cathodic reduction peak under O$_2$ saturated condition suggests the di-oxygen reduction reaction. On contrary no peak is observed for N$_2$ saturated alkaline solution. The cathodic reduction peak is observed at−0.62 V for α−Co(OH)$_2$,−0.30 V for HT-SDS-1 and−0.20 V for HT-SDS-2 respectively. Interestingly, the onset potential for HT-SDS-2 (-0.05 V @ j=0.005 mA) is lower than that of HT-SDS-1 (-0.1 V @ j=0.001 mA) and α−Co(OH)$_2$ (-0.13 V @ J=0.001 mA). Although both HT-SDS-1 and HT-SDS-2 exhibit similar reduction current values for ORR, the later displayed a significant gain in overpotential, which is a crucial parameter for an electrocatalyst. Also, HT-SDS-2 exhibits more than two-fold enhancement in the reduction current value when compared to bare glassy carbon electrode and hence this material is chosen as the best catalyst for further studies. Moreover, the stability of HT-SDS-2 towards ORR in alkaline medium is assessed by measuring the change in reduction current with respect to increasing number of cycles using CV studies. This experiment was carried out by recording CV for 100 cycles in O$_2$ saturated 0.1 M KOH aqueous solution. The corresponding stability data (shown in Figure S7) suggests that 90% of the reduction current is retained upto 60 cycles and 75% retention is noted for 100 cycles recorded at a fixed scan rate of 10 mV/s.These studies clearly demonstrate the good stability of electrocatalyst towards ORR in alkaline medium and vividly demonstrate the potential utility of HT-SDS-2 as an electrocatalyst towards ORR activity in alkaline medium.

In order to understand the kinetics behind ORR and to determine the number of electrons involved in ORR, further experiments were carried out using rotating ring – disc voltammetry. Basically, these studies eliminate the limitations arising from the diffusion of electroactive molecules so that the kinetics associated with electron transfer process will control the reaction. Interestingly this technique is widely used for the investigation of ORR. Here, the disc electrode (glassy carbon) is modified with HT-SDS-2 and LSV experiments were carried out on the disc electrode. Concomitantly, the platinum ring electrode is biased at a potential of 0.5 V and the product analysis due to ORR is studied on the ring. LSV curves were recorded in 0.1 M KOH solution at various rotation speeds starting from 100 rpm to 2500 rpm and the corresponding voltammograms were displayed in figure 9A. It can be observed that the disc current increased systematically with respect to increase in rotation speed due to the enhanced mass transport at the electrode surface and at higher rotations it attains a steady state current. Interestingly the ring current also increases with respect to increasing rotation speeds. Current could be measured at the ring electrode only after ORR proceeds indicating the formation of product as the reduction reaction proceeds and the corresponding current value is detected at the ring electrode. These results suggest the potential use of HT-SDS-2 as an electrocatalyst for ORR. Furthermore, kinetic parameters associated with ORR are determined using Koutecky–Levich (KL) analysis on the basis of following equations.[24]

$$1/J = 1/J_L + 1/J_k = 1/B\omega^{1/2} + 1/J_k \qquad (1)$$

$$B = 0.2nFC_0D^{2/3}\upsilon^{-1/6} \qquad (2)$$

where n is the number of electrons transferred, F is the Faraday's constant, C is the bulk concentration of the electro-active species such as O$_2$ in solution (1.26 × 10^{-6} mol cm^{-3}) at 25°C), D is the diffusion coefficient of O$_2$ (1.93 × 10^{-5} cm^2 s^{-1}), υ is the kinematic viscosity of the solution (1.009 × 10^{-2} cm^2 s^{-1}) and ω is the rotation speed of the electrode (in rpm) respectively.
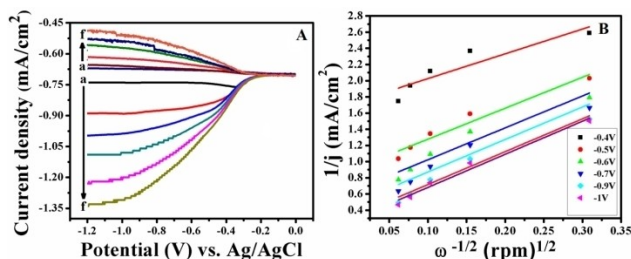

Figure 9. (A) Rotating ring disc electrode (RRDE) voltammetry measurements performed for ORR using HT-SDS-2 as an electrocatalyst in O$_2$ saturated 0.1 M KOH aqueous solution at different rotation rates from 100 rpm to 2500 rpm (a–f). (B) Koutecky–Levich (KL) plots determined for ORR using HT-SDS-2 at different potential values in the range of−0.4 V to−1.0 V. These data points are collected from figure A.

ChemistrySelect

Full Papers
doi.org/10.1002/slct.202002030

**Chemistry
Europe**
European Chemical
Societies Publishing

The number of electrons transferred per O_2 molecule is calculated from the slope value of KL plot and by using the above equations. KL plots obtained at different potential values starting from -0.4 V to -1.0 V are shown in figure 9B. These plots display a good linear behavior and the "n" values are found to be 2.1 to 2.8 at these potential values, indicating the material, HT-SDS-2 predominately exhibits two electron transfer reaction in which the formation of hydrogen peroxide and partially reduced oxygen species are the major products of ORR. Moreover, the percentage yield of hydrogen peroxide formation is calculated using the following equation.[25]

$$HO_2^- \% = 2\ (i_R/N)\ /\ (i_D +\ i_R/N) \tag{3}$$

Where i_D is the disc current, i_R is the ring current and N is the current collection efficiency (0.22 for Pt ring) respectively. Based on the current values measured at both the disc and ring electrodes and by using eq. 3, the percentage yield of H_2O_2 formation is estimated to be $\sim 78\%$. This provides a strong evidence that hydrogen peroxide is a major product during ORR process and the average number of electrons transferred is identified to be 2.3. Nevertheless, these studies clearly indicate that HT-SDS-2 acts as a viable and efficient electro-catalyst for bi-functional applications involving OER and ORR for water splitting reaction in alkaline medium. Moreover, this strategy offers the possibility of tuning electrochemical reaction with the applied potential. For instance, if the potential is tuned in the positive regime this surfactant intercalated cobalt HT layered material shows good OER characteristics and similarly when the potential is reversed in the negative region this displays an excellent catalytic activity for ORR. Among the various surfactant intercalated CoHT materials only SDS interca-lated CoHT alone exhibits good electrocatalytic activity for OER and ORR. In this case particularly HT-SDS-2 displayed a superior performance in terms of higher current density and lower onset potential for OER and ORR in alkaline medium when compared to other systems. This is mainly attributed to the difference in surface area values, intrinsic layered structure and the presence of suitable micropores leading to enhanced accessibility of the electrolyte. Moreover, the adsorption of ions at the catalytically active sites and the accessibility within the layers lead to higher electrocatalytic activity. Finally, these studies clearly demon-strate the potential utility of these materials as bi-functional electrocatalysts for OER and ORR in alkaline medium and hence this material could be used as an electrocatalyst for alkaline fuel cell reactions.

4. Conclusions

In summary, sodium dodecyl sulfate (SDS), trimesic acid (TMA) and sodium laureate (SL) intercalated monometallic cobalt hydrotalcite layered materials are successfully prepared and characterized. The intercalation of organic surfactants into the layer of α-Co(OH)$_2$ is confirmed through FT-IR and powder XRD analyses. XPS studies revealed the presence of Co^{2+} and Co^{3+} oxidation states in these materials. Further, these materials are explored for the electrocatalytic application pertaining to OER

and ORR. Results obtained through the electrochemical studies reveal that SDS intercalated Co-HT material could potentially be used as a bi-functional electro-catalyst for OER and ORR involved in water splitting reaction and similarly could find applications in the field of alkaline fuel cells. Kinetics parame-ters associated with ORR are determined using rotating ring disc voltammetric studies that reveal a predominant 2 electron transfer process leading to the formation of hydrogen peroxide as a major product.

Supporting Information Summary

Experimental procedure, elemental analysis, BJH pore size distribution and deconvoluted XPS spectra of surfactant intercalated α-Co(OH)$_2$ are given in the supporting information. Linear sweep voltammetry plots, electrochemical impedance spectra of surfactant intercalated α-Co(OH)$_2$ along with stability of HT-SDS-2 towards ORR are also provided in the supporting information.

Conflict of Interest

The authors declare no conflict of interest.

[1] a) P. P. Boix, K. Nonomura, N. Mathews, S. G. Mhaisalkar, *Mater. Today* **2014**, *17*,16–23; b) N. T. Whilton, P. J. Vickers, S. Mann, *J. Mater. Chem.* **1997**, *7*, 1623–1629; c) H. Fischer, *Mater. Sci. Eng. C* **2003**, *23*, 763–772; d) U. Costantino, V. Ambrogi, M. Nocchetti, *MicroporousMesoporous Mater.* **2008**, *107*,149–160; e) Yadav, R.; Baskaran, T.; Anjali, K.; Ahmed, M.; Bhosale, S. V.; Joseph, S.; Al-Muhtaseb, A. H.; Singh, G.; Sakthivel, A.; Vinu, A. *Chem. An Asian J.* **2020**, https://doi.org/10.1002/asia.202000651.

[2] a) A. Khan, D. O' Hare, *J. Mater. Chem.* **2002**, *12*, 3191–3198; b) S. P. Newman, W. Jones, *New J. Chem.* **1998**, *22*, 105–115.

[3] a) Y. Park, G. A. Ayoko, R. L. Frost, *J. Colloid Interface Sci.* **2011**, *354*, 292–305; b) G. Kickelbick, *Prog. Polym. Sci.* **2003**, *28*, 83–114; c) C. H. Zhou, *Appl. Clay Sci.* **2011**, *53*, 87–96; d) Y. Kohno, S. Asai, M. Shibata, C. Fukuhara, Y. Maeda, Y. Tomita, K. Kobayashi, *J. Phys. Chem. Solids.* **2014**, *75*, 945–950.

[4] a) B. Zapata, P. Bosch, M. A. Valenzuela, G. Fetter, S. O. Flores, I. R. Cordova, *Mater. Lett.* **2002**, *57*, 679–683; b) D. Sharma, A. Sakthivel, *J. Nanosci. Nanotech.* **2018**, *18*, 381–385; c) T. Baskaran, J. Christopher, M. Mariyaselvakumar, A. Sakthivel, *Eur. J. Inorg. Chem.* **2017**,2396–2405; d) D. Sharma, T. Baskaran, J. Christopher, A. Sakthivel, *Nanosci. Nanotec. Lett.* **2016**, *8*, 360–364; e) A. Sakthivel, N. R. Mahato, T. Baskaran, J. Christopher, *Catal. Commun.* **2015**, *65*, 55–61; f) T. Baskaran, R. Kumaravel, J. Christopher, A. Sakthivel, *RSC Adv.* **2014**, *4*, 11188–11196; g) A. Sreenavya, A. Sahu, A. Sakthivel, *Ind. Eng. Chem. Res.* **2020**, *59*, 11979–11990.

ChemistrySelect

Full Papers
doi.org/10.1002/slct.202002030

Chemistry Europe
European Chemical
Societies Publishing

[5] a) J. P. Purohit, J. E. Huacuja-Sanchez, D. Y. Wang, F. Emmerling, A. Thunemann, G. Heinrich, A. Schonhals, *Macromolecules* **2011**, *44*, 4342–4354; b) X. Lu, R. Ma, Y. Bando, T. Sasaki, *Angew. Chem. Int. Ed*. **2010**, 49, 8253–8256; c) Z. Liu, R. Ma, M. Osada, K. Takada, T. Sasaki, *J. Am. Chem. Soc*. **2005**, *127*, 13869–13874; d) P. Vialat, C. Mousty, C. Taviot-Gueho, G. Renaudin, H. Martinez, J. C. Dupin, E. Elkaim, F. Leroux, *Adv. Funct. Mater*. **2014**, *24*, 4831–4842; e) V. Rives, Layered double hydroxides: Present and Future, Nova Science Publishers, New York, **2001**; f) S. M. Auerbach, K. A. Carrado, P. K. Dutta, Marcel Dekker, Handbook of layered materials. CRC Press, **2004**; g) C. Mousty, F. Leroux, *Recent Pat. Nanotech*. **2012**, *6*, 174–192; h) J. Leng, P. J. Purohit, N. Kang, D.-Y. Wang, J. Falkenhagen, F. Emmerling, A. F. Thunemann, A. Schonhals, *Eur. Polym. J*. **2015**, *68*, 338–354.

[6] a) F. R. Costa, A. Leuteritz, U. Wagenknecht, D. Jehnichen, L. Haeussler, G. Heinrich, *Appl. Clay Sci*. **2008**, *38*, 153–164; b) S. Li, H. Qin, R. Zuo, Z. Bai, *Tribol. Int*. **2015**, *91*, 60–66.

[7] a) Z. Hu, Y. Xie, Y. Wang, L. Xie, G. Fu, X. Jin, Z. Zhang, Y. Yang, H. Wu, *J. Phys. Chem. C*. **2009**, *113*, 12502–12508; b) P. C. Pavan, G. D. Gomes, J. B. Valim, *MicroporousMesoporous Mater*. **1998**, *21*, 659–665.

[8] Z. P. Xu, P. S. Braterman, *J. Phy. Chem. C*. **2007**, *111*, 4021–4026.

[9] K. A. Stoerzinger, M. Risch, B. Han, Y. Shao-Horn, *ACS Catal*. **2015**, *5*, 6021–6031.

[10] L. Wei, X. Gao, D. Xiong, F. Xia, J. Liu, Wei-Guo Song, J. Xu, S. M. Thalluri, M. F. Cerqueira, X. Fu, L.,*Chem. Sci*. **2017**, *8*, 2952–2958.

[11] W. Li, X. Gao, D. Xiong, F. Wei, W. -G Song, J. Xu, L. Liu, *Adv. Energy Mater*. **2017**, *7*, 1602579.

[12] D. Xiong, Q. Zhang, S. M. Thalluri, J. Xu, W. Li, X. Fu, L. Liu, *Chem. Eur. J*. **2017**, *23*, 8749–8755.

[13] W. Li, X. Gao, X. Wang, D. Xiong, P.-P. Huang, W.-G. Song, X. Bao, L. Liu, *J. Power Sources* **2016**, *330*,156–166.

[14] Y. Liang, Y. Li, H. J. Zhou, J. Wang, T. Regier, H. Dai, *Nature Mater*. **2011**, *10*, 780–786.

[15] Y. Zhang, S. Chao, X. Wang, H. Han, Z. Bai, L. Yang, *Electrochim. Acta* **2017**, *246*, 380–390.

[16] Z. J. Jiang, Z. Jiang, *Sci. Rep*. **2016**, *6:*27081, DOI: 10.1038/srep27081.

[17] a) P. Jeevanandam, Y. Koltypin, A. Gendanken, Y. Mastai, *J. Mater. Chem*. **2000**, *10*, 511–514; b) Z. P. Xu, H. C. Zeng, *Chem. Mater*. **1999**, *11*, 67–74; c) Y. Zhu, H. Li, Y. Koltypin, A. Gedanken, *J. Mater. Chem*. **2002**, *12,*729–733.

[18] a) S. Ida, D. Shiga, M. Koinuma, Y. Matsumoto, *J. Am. Chem. Soc*. **2008**, *130*, 14038–14039; b) B. R. Venugopal, C. Shivakumara, M. Rajamathi, *J. Colloid Interface Sci*. **2006**, *294*, 234–239.

[19] a) Y. Hou, H. Kondoh, M. Shimojo, T. Kogure, T. Ohta, *J. Phys. Chem. B*. **2005**, *109*, 19094–19098; b) R. Espinal, E. Taboada, E. Molins, R. J. Chimentao, F. Medina, J. Llorca, *RSC Adv*. **2012**, *2*, 2946–2956; c) M. Kurmoo, *J. Mater. Chem*. **1999**, *9*, 2595–2598; d) M. Wang, J. Ma, C. Chen, X. Zheng, Z. Du, J. Xu, *J. Mater. Chem*. **2011**, *21*, 12609–12612.

[20] F. Cavani, F. Trifiro, A. Vaccari, *Catal. Today*. **1991**, *11*,173–301.

[21] I. Barauskiene, E. Valatka, *Mater Renew Sustain Energy* **2018**, *7*, 1.

[22] a) M. Kurk, M. Jaroniec, *Chem. Mater*. **2001**, *13*, 3169–3183; b) M. L. Occelli, J. P. Olivier, A. Auroux, M. Kalwei, H. Eckert, *Chem. Mater*. **2003**, *15*, 4231–4238.

[23] a) X. Wang, C. Yan, A. Sumboja, J. Yan, P. S. Lee, *Adv. Energy Mater*. **2014**, *4,*1301240–1301247; b) P. Vialat, C. Mousty, C. Taviot-Gueho, G. Renaudin, H. Martinez, J. C. Dupin, E. Elkaim, F. Leroux, *Adv. Funct. Mater*. **2014**, *24*, 4831–4842.

[24] a) P. Ganesan, M. Prabu, J. Sanetuntikul, S. Shanmugam, *ACS Catal*. **2015**, *5*, 3625–3637; b) Y. Liu, D. C. Higgins, J. Wu, M. Fowler, Z. Chen, *Electrochem. Commun*. **2013**, *34*, 125–129; c) Y. Liang, Y. Li, H. Wang, J. Zhou, J. Wang, T. Regier, H. Dai, *Nature Mater*. **2011**, *10*, 780—786;d) H. Fei, R. Ye, G. Ye, Y. Gong, Z. Peng, X. Fan, E. L. G. Samuel, P. M. Ajayan, J. M. Tour, *ACS Nano*. **2014**, *10*, 10837–10843; e) Q. Li, S. Zhang, L. Dai, L. Li, *J. Am. Chem. Soc*. **2012**, *134*, 18932–18935.

[25] a) U. Paulus, T. Schmidt, H. Gasteiger, R. Behm, *J. Electroanal. Chem*. **2001**, *495*, 134–145; b) Z. H. Sheng, L. Shao, J. J. Chen, W. J. Bao, F. B. Wang, X. H. Xia, *ACS Nano*. **2011**, *5*, 4350–4358.